PROCEEDINGS OF SCIENCE

Synthesis and Characterization of Al-doped nanostructured Mg_2Si and Ag_2Se by Pack Cementation and Ball Milling Processes

Nikolaos Sidiropoulos,[α] Iordanis Karagiannis,[α] Vasileios Pavlidis,[α] Aikaterini Teknetzi,[α] Lamprini Malletzidou,[α] Fani Stergioudi,[b] Nikolaos Michailidis,[b] George Vourlias[α] and Dimitrios Stathokostopoulos [α,*]

[a] *Laboratory of Advanced Materials & Devices, School of Physics, Faculty of Sciences, Aristotle University of Thessaloniki*
Thessaloniki, GR-54124, Greece

[b] *Physical Metallurgy Laboratory, Department of Mechanical Engineering, School of Engineering, Aristotle University of Thessaloniki*
Thessaloniki, GR-54124, Greece

E-mail: niksidir@physics.auth.gr, iorkarag@physics.auth.gr, vaspavli@physics.auth.gr, ateknetz@physics.auth.gr, labrinim@auth.gr, fstergio@meng.auth.gr, nmichail@meng.auth.gr, gvourlia@auth.gr, dstat@physics.auth.gr

Thermoelectricity is a green method of energy production by converting waste heat into electricity. Silicides and selenides are candidate materials for thermoelectric applications due to their high performance in their operating temperature range. Additionally, they are composed of abundant and negligibly toxic elements. The current study focuses on the fabrication of alternative thermoelectric materials, aiming to develop compounds with advanced thermoelectric properties. Pure Mg_2Si and Al-doped Mg_2Si samples are synthesized by Pack Cementation, and Ag_2Se powder is produced via Ball Milling (BM). The chosen synthesis methods are suggested as environmentally friendly, fast and economic. The samples were structurally characterized by X-ray diffraction (XRD), while the morphology and the chemical composition were studied by X-ray photoelectron spectroscopy (XPS) and scanning electron microscopy (SEM). In the case of magnesium silicide, the thermoelectric phase was formed without residual traces of the initial elemental powders. The Al addition diffused in the material homogeneously and no secondary phases were developed. Regarding the Ag_2Se powder, α-phase (low temperature) was obtained after 2.5 h of mechanical alloying (BM) the elements. SEM and XPS analysis detected traces of unreacted Ag and Se, indicating that the ball milling process should last longer to achieve a complete reaction between the elements.

11th International Conference of the Balkan Physical Union (BPU11),
28 August - 1 September 2022
Belgrade, Serbia

[*] Speaker

PoS(BPU11)211

1. Introduction

Thermoelectric (TE) technology recovers waste heat providing power generation, while being noiseless, free of carbon emissions and with minimum maintenance requirements. The performance of thermoelectric materials is determined by the dimensionless figure of merit, zT, described as:

$$zT = S^2\sigma T/\kappa \quad \text{(Eq.1)},$$

where σ is the electrical conductivity, $\kappa = \kappa_e + \kappa_L$ is the total thermal conductivity (κ_e and κ_L are the electronic and lattice contributions, respectively), S is the Seebeck coefficient and T is the absolute temperature.

Silicides are regarded as one of the most promising candidates for intermediate- to high-temperature thermoelectric applications due to their attractive TE properties and the high abundance of their constituent elements [1]. Mg_2Si-based materials are economic, non-toxic and light-weight in comparison with other TE materials of the same temperature range, such as $CoSb_3$ and PbTe [2, 3]. The maximum reported zT of these compounds is zT=1.63 at 373 °C [4]. The synthesis of Mg_2Si-based materials is a challenge due to the high affinity of Mg with oxygen. A wide variety of techniques have been employed so far, including solid-state reaction, mechanical alloying (Ball Milling), melting, sputtering and self-propagating high-temperature synthesis (SHS), commonly followed by spark plasma sintering, hot-press or plasma activated sintering [5-11]. The afore-mentioned methods have some drawbacks. Some of them require precision and state of the art equipment to be carried, such as sputtering or SHS. For solid state reaction, it is difficult to synthesize powders without secondary phases and the process is often time and energy-consuming. Because of the high vapor pressure of Mg, it is difficult to control the composition during the melting methods. Finally, Mg_2Si prepared by mechanical alloying is frequently contaminated and is likely to form aggregates.

Ag-Se alloys are getting increasing attention for low-temperature thermoelectric applications. Specifically, Ag_2Se possesses ultra-low lattice thermal conductivity, high power factor around room temperature and a narrow band gap of 0.15 eV. In other words, this compound is a "phonon liquid electron crystal" (PLEC). The maximum reported zT for Ag_2Se is close to that of the commercial Bi_2Te_3 ingots, reaching the peak value zT=1.2 near room temperature [12]. The toxicity and/or scarcity of Bi and Te are the main reason that new low-temperature TE materials, such as Ag-Se alloys, need to be developed. Various synthesis techniques have been applied to prepare Ag_2Se. The most common method for synthesizing polycrystalline ingots is zone-melting (ZM) [13]. Furthermore, ball milling and chemical methods (e.g. hydrothermal reaction, colloidal synthesis) [14, 15] are frequently used to produce powders with refined grain size and morphology. Combining hot pressing (HP) or spark plasma sintering (SPS) with ball milling is an effective method for improving the TE performance. This is accomplished by reducing the thermal conductivity through the increased phonon scattering on very fine grains.

The current work focuses on the synthesis of Al doped Mg_2Si powder ($Mg_{2.18-x}SiAl_x$, x = 0, 0.01) and Ag_2Se powder, which are prepared by pack cementation and ball milling technique, respectively. Both methods are low-cost, simple and environmentally friendly, as no toxic by-products are released during the synthesis process. Aluminum dopant was selected for enhancing the TE properties of n-type Mg_2Si because of its low price and ecological character

[16, 17]. The main effect of Ball Milling method on Ag_2Se is the modification of the defect concentration, which is achieved through the mechanical energy gained from the collisions with the balls and the conversion to thermal energy. The morphological changes and the introduction of defects are responsible for the optimization of the TE properties. The synthesized $Mg_{2.18-x}SiAl_x$ and Ag_2Se powders were studied regarding their structure and composition, and the preparation routes were evaluated.

2. Experimental section

The method of pack cementation (PC), employed for the synthesis of nanostructured Mg_2Si powder and other thermoelectric silicides, has been described in detail elsewhere [18-20]. In brief, a homogeneous powder mixture of Mg, Si and a halide salt activator is prepared. The procedure is divided in two stages. During the first stage of thermochemical reaction, the activator thermally decomposes, and the halide products favourably react with Mg (donor). The gaseous metal halides are transferred to the surface of Si (base material) where they decompose depositing the donor in a highly reactive form. The byproducts react again recycling the chemical process, until the donor is totally consumed. Subsequently, the step of solid-state diffusion follows, with the Mg atoms predominantly moving inwards into Si grains [18, 21].

For the synthesis of Al doped Mg_2Si with pack cementation procedure, powders of Si (purity 99.5%, ≤44 μm), Mg (purity 99.5%, ≤44 μm) and Al (purity 99.5%, ≤44 μm) were weighed according to the stoichiometric compositions $Mg_{2.18-x}SiAl_x$ (x = 0 and 0.01) and they were homogeneously mixed along with NH_4Cl; the latter was used as the activator. The excess of Mg powder is used in order to compensate for the loss during the synthesis [22], while the concentration of NH_4Cl was constant at 3 wt%. The powder mixtures were placed in ceramic crucibles and with a lid having a hole before being placed in the furnace. The heating temperature was 650 °C, while the holding time was 5 h (Table 1). The whole process took place under argon flow 99.98% in order to protect the samples from oxidation. Additionally, the synthesis chamber was purged before the experimental procedure, using a rotary vacuum pump up to 2×10^{-2} mbar. The Mg_2Si-based powders were hot pressed to pellets up to 700 °C, under 85 MPa and inert atmosphere for 4 h in a graphite die (diameter 13 mm). The density of the pellets was ~85% of the theoretical value (1.99 gr/cm^3). The density (q) was estimated from mass (m) and volume (V) measurements using the equation q=m/V.

Code name	***Theor. Comp.***	***Temperature PC (°C)***	***Time PC (h)***	***Atmosphere PC***
MS0	$Mg_{2.18}Si$	650	5	Argon
MS1	$Mg_{2.17}SiAl_{0.01}$	650	5	Argon
Code name	***Theor. Comp.***	***Rotational speed BM (rpm)***	***Time BM (h)***	***Atmosphere BM***
AS	Ag_2Se	500	2.5	Argon

Table 1: *Experimental conditions of the synthesized samples and given code names.*

For the synthesis of Ag_2Se, elemental powders of Ag (purity 99.9%, ≤44 μm) and Se (purity 99.5%, ≤44 μm), weighed in the appropriate stoichiometric ratio (2:1), were placed into an agate milling vessel with twenty-five agate balls (10 mm diameter). The powders were blended in a high-energy ball mill for 2.5 h (with a 15 min interval every 30 min) at a speed of 500 rpm (Table 1). The ball milling jar was sealed with inert gas (argon), to prevent oxidation

which could occur during a long milling process in air atmosphere. The synthesis of ball milling (BM) was carried out with a FRITSCH Planetary Micro Mill, model PULVERISETTE 7.

Structural and chemical characterization of the synthesized materials was carried out employing different techniques. The phase identification was performed for pellets and powders by X-ray diffraction (XRD) analysis, using a 2-cycle Rigaku Ultima$^+$ powder X-ray diffractometer, with Cu K_a radiation and operating at 40 kV/30 mA. The data were collected with a step of 0.05° and scan speed of 1.5 s/step. Scanning Electron Microscopy (SEM) measurements were performed using a JEOL JMS-390LV electron microscope, equipped with an OXFORD INCA 300 energy dispersive X-ray spectrometer (EDS), in order to acquire information regarding the chemical composition and morphology of the powders and pellets. The chemical state of the constituent elements and the chemical composition of the surface were studied by X-ray photoelectron spectroscopy (XPS) using a KRATOS Axis Ultra^{DLD} system equipped with a monochromated Al K_a (1484.6 eV) X-ray source, a hemispherical sector electron analyzer and a multichannel electron detector under ultra-high vacuum conditions (10^{-9} Torr). Calibration of the spectra achieved with the C 1s peak at 284.6 ± 0.2 eV (binding energy) for the C-C bonds due to the contamination of atmosphere.

3. Results and Discussion

3.1. Characterization of Mg_2Si

The XRD patterns in Fig. 1 show the Pack Cementation Mg-Si powder mixture with Al. The majority of the peaks corresponds to Mg_2Si as the main phase (2θ=40.12°), possessing antifluorite crystallographic structure (CaF_2) and Fm3m space group.

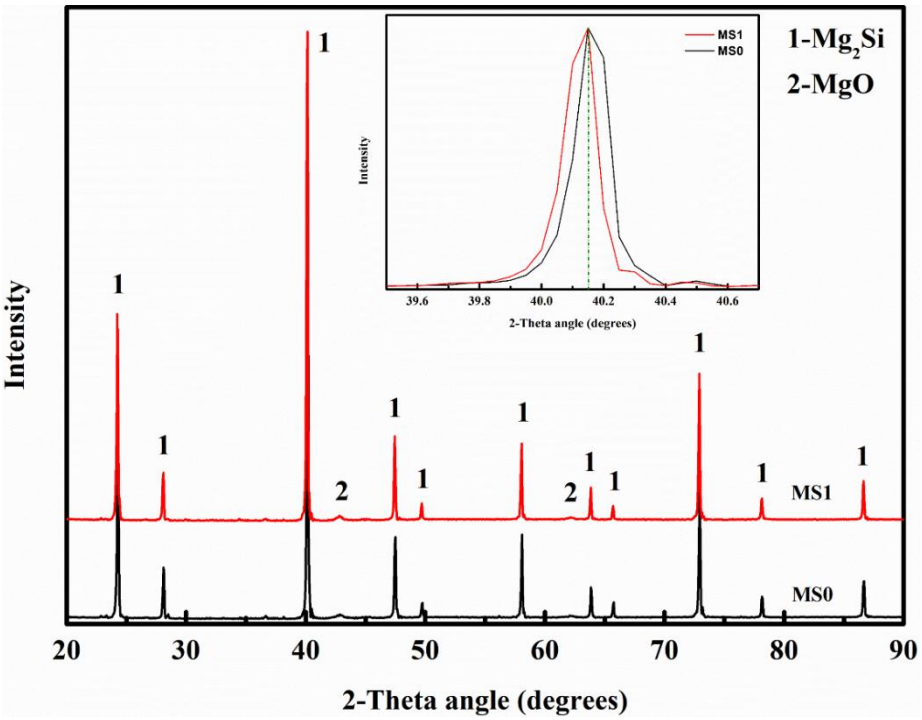

Figure 1: *XRD patterns of Mg-Si powder with varying Al concentration. The inset presents the region around to (2 2 0) peak.*

The presence of a small peak of MgO (2θ=36.62°) is also detected due to high affinity of magnesium with oxygen, as MgO exhibits negative change in free energy the value of which is one of the highest among the metals. (ΔG=-1138kJ/mol at room temperature) [23]. Via XRD pattern fitting and Rietveld refinement (Program FullProf.2K-Version 7.20), the weight percentage of MgO is quantified about 5%, which is in good agreement with literature [24]. The peaks were indexed by Mg_2Si PDF #65-2988 and MgO PDF #45-09 [25]. Several studies refer that the added Al substitutes the Mg atoms in the lattice. Other studies claim that under specific circumstances, Al substitute on Si atoms [26, 27], as the formation energy is lower than substituting at Mg sites. Particularly, Zwolenski et al. refers that the site preference can tentatively be predicted from, e.g., the Korringa–Kohn–Rostoker method with the coherent potential approximation (KKR-CPA) formation energy. In this case of Al-doped Mg_2Si, Al substitutes at the Si site [28]. Due to the larger atomic radius of aluminum in relation to silicon, an increase in the lattice constant is expected [29]. Consequently, the XRD pattern of sample MS1 will be shifted to lower angles compared to MS0. A magnification of 2θ-angle in Fig. 1 (inset diagram) verifies the theoretically expected observation. Castillo et al. estimated the lattice constant of undoped Mg_2Si to be 6.349 ± 0.002 Å [30]. The lattice parameter of the samples was calculated by applying Bragg's equation [31] for all peaks from XRD pattern. The results are included in Table 2.

Sample	***Average Lattice Parameter (Å)***	***Average Crystallite Size (nm)***
MS0	6.349	72.00 ± 1.15
MS1	6.350	71.21 ± 1.12

Table 2: *Crystallographic quantification of Mg-Si powder with aluminum doping.*

The crystallite size was determined by applying the Debye – Scherrer equation (given below) for the predominant peaks and the results are presented in Table 2:

$$L = \frac{K \cdot \lambda}{\delta(2\theta) \cdot cos\theta} \text{ (Eq. 2)},$$

where K is Scherrer constant (assumed as K=0.89 for spherical shape), L is the crystallite size, θ is the position of the peak and δ(2θ) is the integral breadth of the reflection which is corrected for the instrumental broadening. The Al doped material presents broader peaks, which is attributed to the decrease of the crystalline size and the introduced lattice strain; this was caused from the introduction of aluminum and the thermochemical diffusion process. Furthermore, the peak broadening is considered to be affected from crystallite size, while strain broadening is neglected [32], which is in agreement with Al doped materials [33].

The microstructure images of hot pressed $Mg_{2.18-x}SiAl_x$ powders are shown in Fig. 2 (a-b). The chemical composition was determined by EDS analysis. Figure 2 (a) depicts the SEM image of the MS0 pellet, and the results of the EDS analysis revealed that the sample contains 65 ± 3 at% Mg and 35 ± 3 at% Si. Figure 2 (b) presents the elemental mapping for the MS1 sample corresponding to a representative area denoted with the dashed rectangle. The EDS elemental mapping of MS1 revealed a homogeneous Mg-Si content of 66 ± 3 at% Mg and 33 ± 3 at% Si for the whole area, which corresponds to Mg_2Si thermoelectric phase. No other

secondary phases and unwanted impurities were detected in the material. Tani et al. reported that the solubility limit of aluminum in Mg_2Si is around 0.15 at%. Thus, it is confirmed that no preferred phase is formed between aluminum and the basic elements [34].

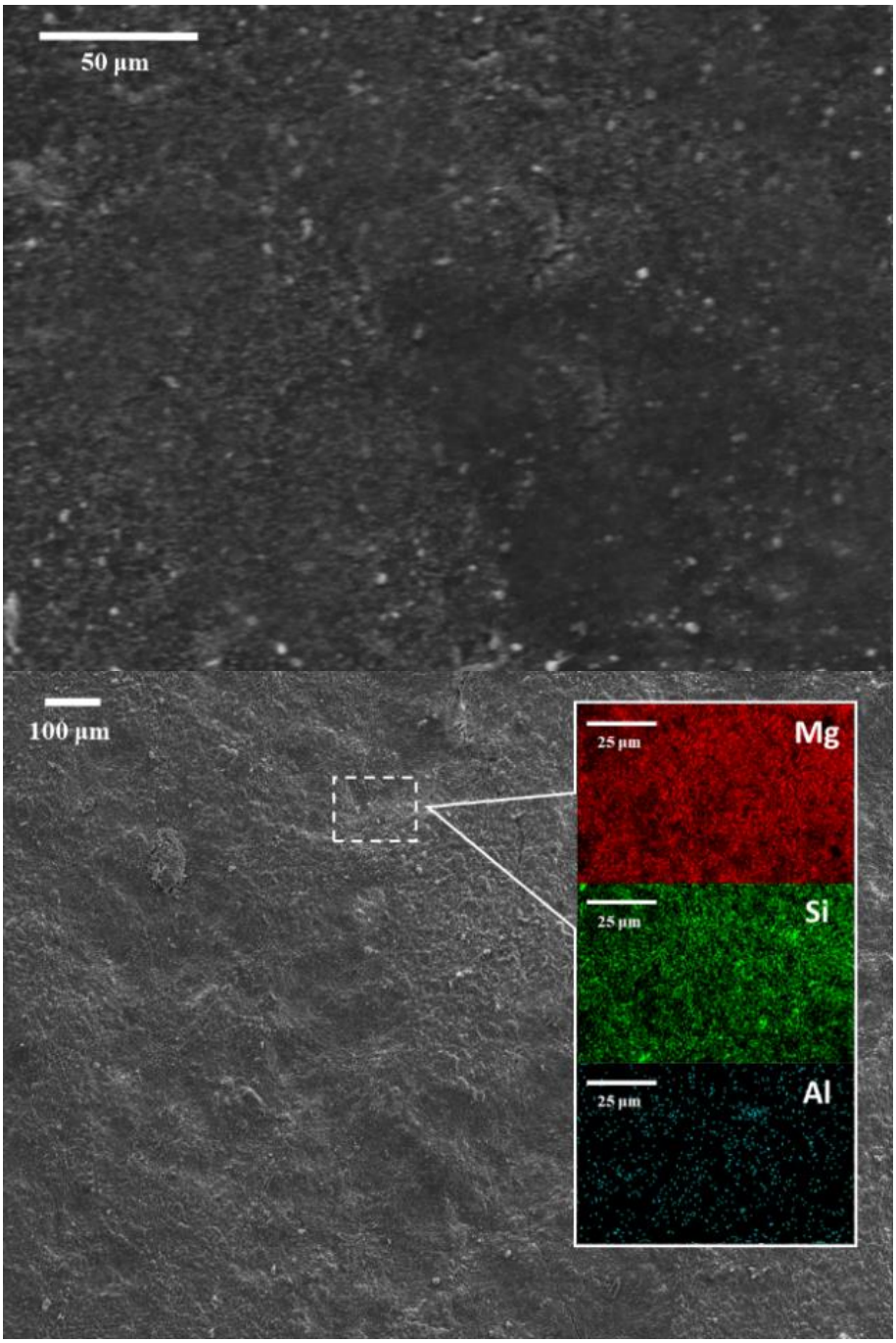

Figure 2: *SEM images of the hot-pressed samples a) MS0 and b) MS1 with the corresponding elemental mappings.*

3.2. Characterization of Ag_2Se

According to Ferhat and Nagao [35], α-Ag_2Se (low-temperature phase) is the most stable

phase in the phase diagram of Ag-Se [36]. This phase possesses an orthorhombic structure (a = 4.333 Å, b = 7.062 Å and c = 7.764 Å) at room temperature [37, 38]. Above ~130 °C, Ag_2Se undergoes a first order phase transformation to β-Ag_2Se body-centered cubic structure (a = 5.043 Å) [39]. The phase composition and the crystallographic structure of the synthesized Ag-Se material were determined by XRD analysis. Figure 3 shows the XRD pattern of the Ag_2Se powder prepared by BM Ag and Se in a stoichiometric ratio of 2:1 for 2.5 h. The majority of the peaks are well indexed by the pattern that is most commonly reported in literature (PDF# 24-1041) [25], identifying the orthorhombic structure (α-Ag_2Se) with a space group of $P2_12_12_1$ [40–42]. According to the XRD analysis, the synthesized material seems to be of a single-phase, as there is no indication of excess Ag or Se, and it is probably stoichiometric. The lattice parameters were calculated by applying Bragg's Law [31] and the d-spacing equation is given below:

$$\frac{1}{d^2} = \frac{h^2}{a^2} + \frac{k^2}{b^2} + \frac{l^2}{c^2}, \text{(Eq. 3)}$$

The calculated values are a =4.331 Å, b =7.059 Å and c =7.761 Å. The experimental parameter values are consistent with those of PDF #24-1041 and previously reported experimental values [25, 43]. The crystallite size was determined by applying the Debye – Scherrer equation (Eq. 2) for the six most predominant peaks: (1 1 2), (1 2 1), (2 0 1), (1 1 3), (0 3 1) and (0 1 3) located at 2θ = 33.48°, 34.75°, 43.32°, 42.64°, 36.99° and 40.01°, respectively. The crystallite size was calculated to be ~42 nm, which is in agreement with the results of previous reports employing the same synthesis method [44].

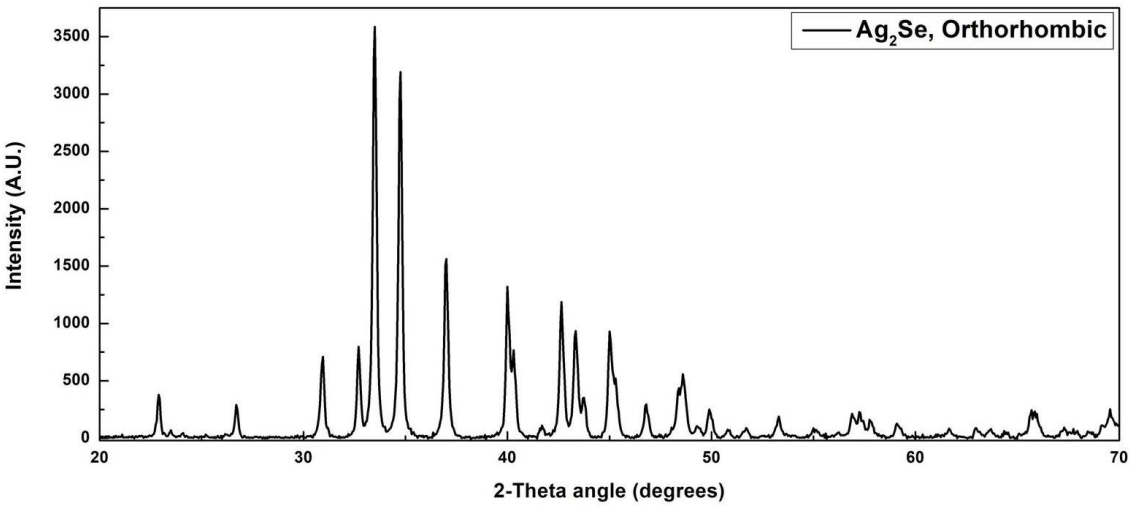

Figure 3: *The XRD pattern of the Ag_2Se powder, indexed by PDF# 24-1041*[25].

Ag_2Se powder was morphologically characterized by SEM analysis and a representative image of the powder is shown in Fig. 4. The grains have irregular shapes with an average size of ~20 μm. The chemical composition was determined by EDS analysis. Figure 4 depicts some representative EDS point measurements, and the results are included in Table 3. In general, the measured composition is fairly close to the nominal one and corresponds to Ag_2Se phase. Interestingly, a different finding is spotted in spectrum #3, at which an excess of Ag can be

detected. Few points with similar composition were sparsely found in other areas too, probably indicating the presence of unreacted Ag traces. The amount of the pure Ag is very limited and below the detection limit of XRD analysis. Also, in Fig. 4, the elemental maps of a representative area (denoted with the dashed rectangle) are presented. In general, the whole region is homogenous regarding the Ag and Se concentration, and there is no evidence of secondary phases.

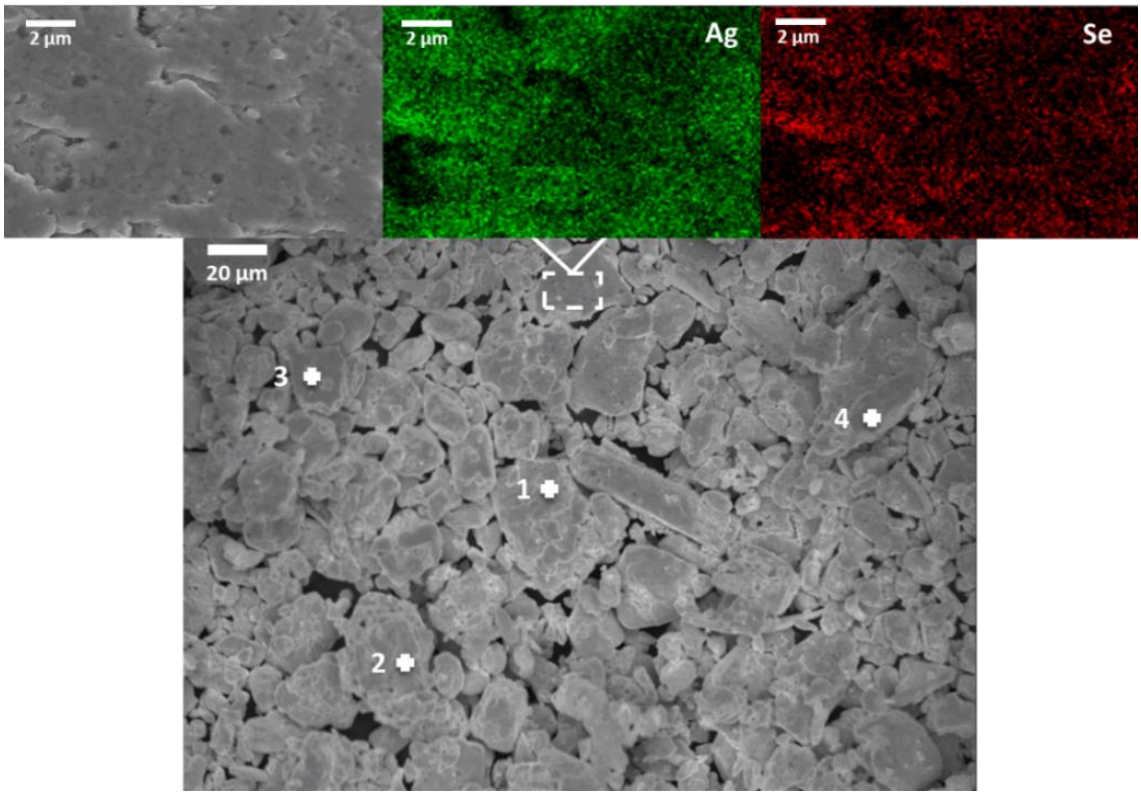

Figure 4: *SEM image of the Ag_2Se powder and the corresponding elemental maps of the area denoted with the dashed rectangle.*

Spectrum Label	***1***	***2***	***3***	***4***
Se (at%)	33.58	34	20.43	36.8
Ag (at%)	66.42	66	79.57	63.2

Table 3: *Percentage concentration of the elements in Ag_2Se powder determined by EDS point measurements.*

The surface of Ag_2Se powder was further examined regarding its chemical composition and the chemical state of the constituent elements by XPS analysis. Figure 5 (a) shows the wide scan and Fig. 5 (b-c) depicts the high resolution (HR) spectra for Ag 3d and Se 3d core levels, respectively. The curve-fitting of the spectra in this figure was performed using the least possible number of components required for a good fitting.

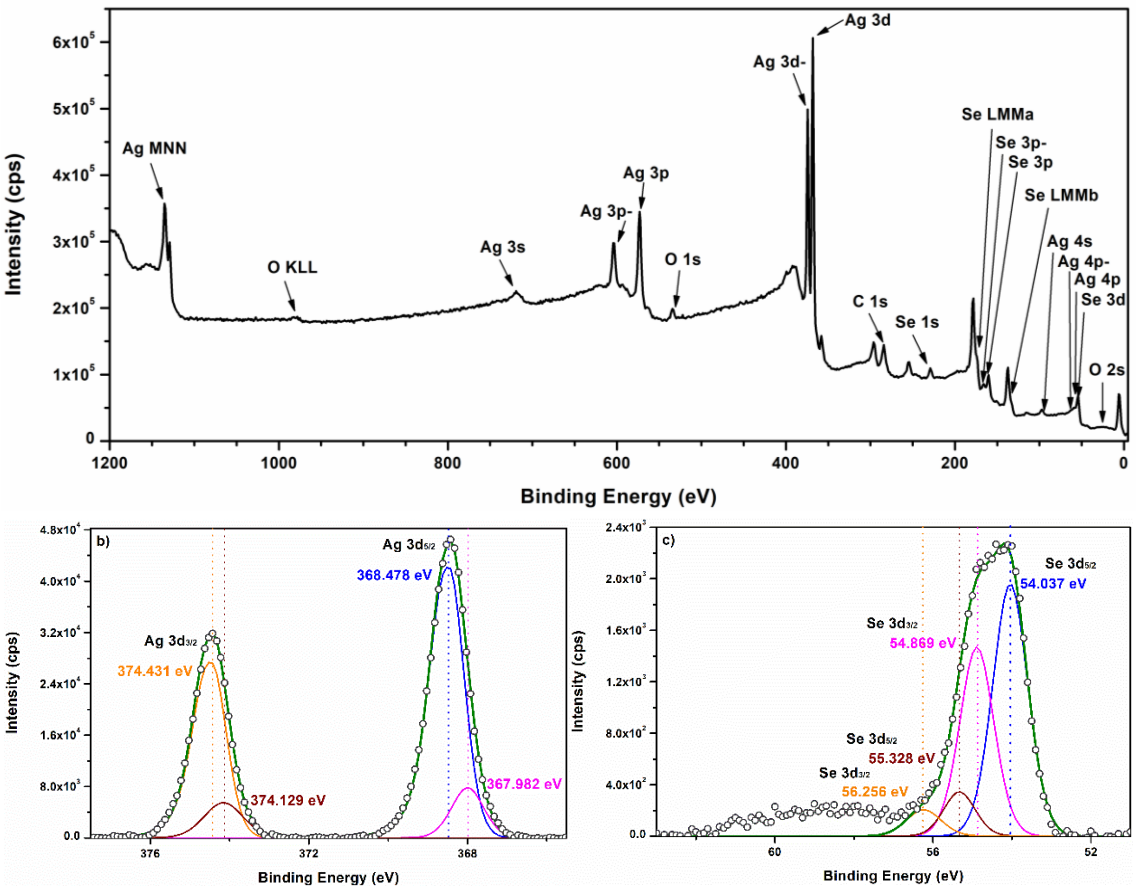

Figure 5: *a) XPS widescan of Ag_2Se powder, b) High Resolution XPS of Ag 3d core level and c) High Resolution XPS of Se 3d core level.*

In Fig. 5 (b) the peaks from Ag 3d orbitals are demonstrated along with their analysis. The broad Ag $3d_{5/2}$ and $3d_{3/2}$ peaks located at 368.425 eV and 374.425 eV, respectively, can be fitted by a pair of sub-peaks each one of them. The components at 368.478 eV and 374.431 eV of $3d_{5/2}$ and $3d_{3/2}$ orbitals, respectively, can be ascribed to Ag^+ oxidation state, which is present in Ag_2Se compound [45, 46]. The sub-peaks at 367.982 eV and 374.129 eV of $3d_{5/2}$ and $3d_{3/2}$ orbitals, respectively, exhibit an energy difference of 6 eV, identifying the spin-orbit splitting of metallic Ag and confirming the presence of the Ag^0 oxidation state in the sample [47–49]. Combining the results from SEM and XPS analyses, the existence of limited metallic silver in the powder is confirmed. The 84.1% of the total Ag bonds are occupied in Ag_2Se compound and only the 15.9% originates from metallic silver. However, this highlights the need for a longer duration of BM in order to attain a single-phase powder without any metallic Ag traces. In Fig. 5 (c) the peaks from Se 3d orbitals are depicted. The Se $3d_{5/2}$ and $3d_{3/2}$ peaks overlap [50] and for each one of them two components were used to fit the curve. The pair of $3d_{5/2}$ and $3d_{3/2}$ peaks located at 54.037 eV and 54.869 eV, respectively, are attributed to the Se^{-2} oxidation state that is present in Ag_2Se [50]. The sub-peaks located at 55.328 eV and 56.256 eV, respectively, demonstrate an energy separation equal to 0.86 eV, confirming the existence of the Se^0 oxidation state and, thus, the presence of metallic Se in the powder [51]. The 86.8% of the total Se bonds are occupied in Ag_2Se compound and only the 13.2% originates from metallic selenium. It is noted that the amount of metallic Se was too limited to be detected by XRD or SEM analysis. Additionally,

quantitative analysis was performed by XPS on the surface of the powder. According to the results listed in Table 4, the powder is slightly nonstoichiometric due to the excess of Ag leading to a Ag:Se ratio equal to 2.9:1, approximately. This observation may be caused by the ball milling prosses itself; an amount of Se is lost. Carbon and oxygen are due to exposure of the Ag_2Se sample to the atmosphere before the XPS measurement.

Peak	***Atomic Conc. %***
C 1s	50.52
O 1s	7.15
Ag 3d	29.97
Se 3d	12.36

Table 4: *XPS quantification report of the Ag_2Se sample.*

4. Conclusions

This study is focused on the formation of thermoelectric materials synthesized by environmentally friendly, fast and economic methods. Thermoelectric pure and Al-doped Mg_2Si and Ag_2Se were synthesized via Pack Cementation and Ball Milling, respectively. All samples were characterized regarding their structure and morphology. The XRD analysis confirmed that the thermoelectric phases were formed in all samples. The average crystallite size was calculated to be about 72, 71 and 42 nm for Mg_2Si, Al-doped Mg_2Si and Ag_2Se, respectively. Considering the Mg-Si XRD analysis, the detection of a small amount of MgO was inevitable due to the high affinity of magnesium with oxygen. According to SEM analysis, the stoichiometric ratio of the thermoelectric phases of all the samples was confirmed. The EDS elemental mapping performed on the Al-doped Mg_2Si pellet revealed homogenous diffusion of Al in the Mg_2Si matrix without the presence of any discrete secondary phase. The grains of the Ag_2Se powder had an irregular shape with an average size of ~20 μm. EDS point measurements detected a limited excess of Ag. XPS analysis detected traces of both metallic Ag and Se, apart from the Ag_2Se compound. This result indicates that the duration of the Ball Milling should be longer than 2.5 h to achieve a complete reaction between the elements.

Acknowledgments

This research was carried out as part of the project «Design and implementation of innovative lift's air-conditioning systems by using thermoelectric devices» (Project code: KMP6-0074109) under the framework of the Action «Investment Plans of Innovation» of the Operational Program «Central Macedonia 2014 2020», that is co-funded by the European Regional Development Fund and Greece.

References

[1] Q. Zhang, Y. Zheng, X. Su, K. Yin, X. Tang, C. Uher, *Enhanced power factor of $Mg_2Si_{0.3}Sn_{0.7}$ synthesized by a non-equilibrium rapid solidification method*," *Scr Mater* **96 (**2015) 414-418 [doi.org/10.1016/j.scriptamat.2014.09.009].

[2] K. Biswas, J. He, I. Blum, C. Wu, T. P. Hogan, D. N. Seidman, V. P. Dravid, M. G. Kanatzidis, *High-performance bulk thermoelectrics with all-scale hierarchical architectures*, *Nature* **489** (2012) [doi.org/10.1038/nature11439].

[3] V. K. Zaitsev, M. I. Fedorov, E. A. Gurieva, I. S. Eremin, P. P. Konstantinov, A. Yu. Samunin, M. V. Vedernikov, *Highly effective $Mg_2Si_{1-x}Sn_x$ thermoelectrics*, *Phys Rev B Condens Matter Mater Phys* **74** (2006) [doi.org/10.1103/PhysRevB.74.045207].

[4] H. Ning, G. D. Mastrorillo, S. Grasso, B. Du, T. Mori, C. Hu, Y. Xu, K. Simpson, G. Maizzab, M. J. Reece, *Enhanced thermoelectric performance of porous magnesium tin silicide prepared using pressure-less spark plasma sintering*, *J Mater Chem A Mater* **3** (2015) [doi.org/10.1039/C5TA03473F].

[5] D. Cederkrantz, N. Farahi, K. A. Borup, B. B. Iversen, M. Nygren, A. E. C. Palmqvist, *Enhanced thermoelectric properties of Mg_2Si by addition of TiO_2 nanoparticles, J Appl Phys* **111** (2012) [doi.org/10.1063/1.3675512].

[6] J. I. Tani, H. Kido, *Fabrication and thermoelectric properties of Mg2Si-based composites using reduction reaction with additives*, *Intermetallics (Barking)* **32** (2013) 72–80 [doi.org/10.1016/j.intermet.2012.08.026].

[7] Q. Zhang, W. Liu, C. Liu, K. Yin, X. F. Tang, *Thermoelectric Properties of $Mg_2(Si_{0.3}Sn_{0.7})_{1-y}Sb_y$ Solid Solutions Doped with Co as CoSi Secondary Phase*, *J Electron Mater,* **43** (2014), [doi.org/10.1007/s11664-014-3002-z].

[8] Q. S. Meng, W. H. Fan, R. X. Chen, Z. A. Munir, *Thermoelectric properties of Sc- and Y-doped Mg_2Si prepared by field-activated and pressure-assisted reactive sintering*, *J Alloys Compd* **509** (2011) [doi.org/10.1016/j.jallcom.2011.05.033].

[9] T. Dasgupta, C. Stiewe, R. Hassdorf, A. J. Zhou, L. Boettcher, E. Mueller, *Effect of vacancies on the thermoelectric properties of $Mg_2Si_{1-x}Sb_x$ ($0 \leq x \leq 0.1$)*," *Phys Rev B Condens Matter Mater Phys* **83** (2011) [doi.org/10.1103/PhysRevB.83.235207].

[10] B. Zhang *et al.*, *Electrical transport characterization of Al and Sn doped Mg_2Si thin films*, *J Alloys Comp d* **720** (2017) 156–160 [doi.org/10.1016/j.jallcom.2017.05.224].

[11] Q. Zhang *et al.*, *Phase segregation and superior thermoelectric properties of $Mg_2Si_{1-x}Sb_x$ ($0 \leq x \leq 0.025$) prepared by ultrafast self-propagating high-temperature synthesis*, *ACS Appl Mater Interfaces* **8** (2016) [doi.org/10.1021/acsami.5b11063].

[12] J. Andres Perez-Taborda, O. Caballero-Calero, L. Vera-Londono, F. Briones, M. Martin-Gonzalez, *High Thermoelectric zT in n-Type Silver Selenide films at Room Temperature*, *Adv Energy Mater* **8** (2018) [doi.org/10.1002/AENM.201702024].

[13] M. Jin, J. Liang, P. Qiu, H. Huang, Z. Yue, L. Zhou, R. Li, L. Chen, X. Shi, *Investigation on Low-Temperature Thermoelectric Properties of Ag_2Se Polycrystal Fabricated by Using Zone-Melting Method*, *J Phys Chem Lett* **12** (2021) [doi.org/10.1021/acs.jpclett.1c02139].

[14] C. Lee, Y. H. Park, H. Hashimoto, *Effect of nonstoichiometry on the thermoelectric properties of a Ag_2Se alloy prepared by a mechanical alloying process*, *J Appl Phys* **101** (2007) [doi.org/10.1021/acs.jpclett.1c02139].

[15] R. Santhosh, R. Abinaya, J. Archana, S. Ponnusamy, S. Harish, M. Navaneethan, *Controlled grain boundary interfaces of reduced graphene oxide in Ag_2Se matrix for low lattice thermal conductivity and enhanced power factor for thermoelectric applications*, *J Power Sources* **525** (2022) [doi.org/10.1016/j.jpowsour.2022.231045].

[16] S. Battiston *et al.*, *Synthesis and Characterization of Al-Doped Mg_2Si Thermoelectric Materials*, *J Electron Mater* **42** (2013) [doi: 10.1007/S11664-013-2482-6].

[17] S. W. You, K. H. Park, I. H. Kim, S. M. Choi, W. S. Seo, S. U. Kim, *Solid-State Synthesis and Thermoelectric Properties of Al-Doped Mg_2Si*, *J Electron Mater* **41** (2011) [doi.org/10.1007/S11664-011-1786-7].

[18] D. Stathokostopoulos, A. Teknetzi, E. Tarani, D. Karfaridis, K. Chrissafis, E. Hatzikraniotis, G. Vourlias, *Synthesis and characterization of nanostructured Mg_2Si by pack cementation process*, *Results in Materials* **13** (2022) [doi.org/10.1016/j.rinma.2021.100252].

[19] D. Stathokostopoulos, D. Chaliampalias, E. Tarani, A. Theodorakakos, V. Giannoulatou, G.S. Polymeris, E. Pavlidou, K. Chrissafis, E. Hatzikraniotis, K.M. Paraskevopoulos, G. Vourlias *Formation of the Thermoelectric Candidate Chromium Silicide by Use of a Pack-Cementation Process*, *J Electron Mater* **43** (2014) [doi.org/10.1007/s11664-014-3100-y].

[20] A. Teknetzi, E. Tarani, E. Symeou, D. Karfaridis, D. Stathokostopoulos, E. Pavlidou, T. Kyratsi, E. Hatzikraniotis, K. Chrissafis, G.Vourlias, *Structure and thermoelectric properties of higher*

manganese silicides synthesized by pack cementation, *Ceram Int*, **47** (2021) 243–251 [doi.org/10.1016/j.ceramint.2020.08.127].

[21] D. Stathokostopoulos, E. C. Stefanaki, M. Ioannou, G. S. Polymeris, D. Chaliampalias, E. Pavlidou, Th. Kyratsi, K. M. Paraskevopoulos, G. Vourlias, E. Hatzikraniotis, *Thermoelectric properties of Mg_2Si coatings deposited by pack cementation assisted process on heavily doped Si substrates*, P*hys Status Solidi* **211** (2014) [doi.org/10.1002/PSSA.201300140].

[22] Q. Zhang *et al.*, *Phase segregation and superior thermoelectric properties of $Mg_2Si_{1-x}Sb_x$ ($0 \leq x \leq 0.025$) prepared by ultrafast self-propagating high-temperature synthesis*, *ACS Appl Mater Interfaces* **8** (2016) [doi.org/10.1021/acsami.5b11063].

[23] D. Eliezer, H. Alves, *Corrosion and Oxidation of Magnesium Alloys*, *Handbook of Materials Selection*, (2007) 267–291 [doi.org/10.1002/9780470172551.ch9].

[24] S. Battiston *et al.*, *Synthesis and Characterization of Al-Doped Mg_2Si Thermoelectric Materials*, *J Electron Mater* **42** (2013) [doi.org/10.1007/S11664-013-2482-6].

[25] International Centre for Diffraction Data (ICDD) (Formerly Joint Committee on Powder Diffraction Standards- JCPDS), *Powder Diffraction File (PDF)*, 2003.

[26] B. Zhang *et al.*, *Electrical transport characterization of Al and Sn doped Mg_2Si thin films*, *J Alloys Compd* **720** (2017) 156–160 [doi.org/10.1016/j.jallcom.2017.05.224].

[27] J. Tani, H. Kido, *First-principles and experimental studies of impurity doping into Mg_2Si*, *Intermetallics (Barking)* **16** (2008) 418–423 [doi.org/10.1016/j.intermet.2007.12.001].

[28] P. Zwolenski, J. Tobola, S. Kaprzyk, *A Theoretical Search for Efficient Dopants in Mg_2X (X = Si, Ge, Sn) Thermoelectric Materials*, *J Electron Mater* **40** (2011) 889–897 [doi.org/10.1007/s11664-011-1624-y].

[29] W. M. Haynes, *Handbook of Chemistry and Physics*, 95th edition. CRC Press, 2014.

[30] G. Castillo-Hernandez, M. Yasseri, B. Klobes, S. Ayachi, E. Müller, J. de Boor, *Room and high temperature mechanical properties of Mg_2Si, Mg_2Sn and their solid solutions*," *J Alloys Compd* **845** (2020) [doi.org/10.1016/j.jallcom.2020.156205].

[31] W. H. Bragg, W. L. Bragg, *The reflection of X-rays by crystals*, *Proceedings of the Royal Society of London. Series A, Containing Papers of a Mathematical and Physical Character* **88** (1913) 428–438 [doi.org/10.1098/rspa.1913.0040].

[32] M. Ioannou, E. Hatzikraniotis, Ch. Lioutas, Th. Hassapis, Th. Altantzis, M. Paraskevopoulos, Th. Kyratsi*, Fabrication of nanocrystalline Mg_2Si via ball milling process: Structural studies*, *Powder Technol* **217** (2012) 523–532 [doi.org/10.1016/j.powtec.2011.11.014].

[33] P. Vivekanandhan, R. Murugasami, S. Appu Kumar, S. Kumaran, *Structural features and thermoelectric properties of spark plasma assisted combustion synthesised Magnesium silicide doped with Aluminium*, *Mater Chem Phys* **241** (2020) [doi.org/10.1016/j.matchemphys.2019.122407].

[34] J. I. Tani, H. Kido, *Thermoelectric properties of Bi-doped Mg_2Si semiconductors*, *Physica B Condens Matter* **364** (2005) 218–224 [doi.org/10.1016/j.physb.2005.04.017].

[35] M. Ferhat, J. Nagao, *Thermoelectric and transport properties of β-Ag_2Se compounds*, *J Appl Phys* **88** (2000) 813–816 [doi.org/10.1063/1.373741].

[36] I. Karakaya, W. T. Thompson, *The Ag-Se (Silver-Selenium) system*, *Bulletin of Alloy Phase Diagrams* **11** (1990) 266–271 [doi.org/10.1007/bf03029297].

[37] J.A. Perez-Taborda, O. Caballero-Calero, L. Vera-Londono, F. Briones, M. Martin-Gonzalez, *High Thermoelectric zT in n-Type Silver Selenide films at Room Temperature*, *Adv Energy Mater*, **8** (2018) [doi.org/10.1002/aenm.201702024].

[38] W. Mi, P. Qiu, T. Zhang, Y. Lv, X. Shi, L. Chen, *Thermoelectric transport of Se-rich Ag_2Se in normal phases and phase transitions*, *Appl Phys Lett* **104** (2014) [doi.org/10.1063/1.4870509].

[39] M. Jin *et al.*, *Investigation on Low-Temperature Thermoelectric Properties of Ag_2Se Polycrystal Fabricated by Using Zone-Melting Method*," *J Phys Chem Lett* **12** (2021) [doi.org/10.1021/acs.jpclett.1c02139].

[40] R. Santhosh, R. Abinaya, J. Archana, S. Ponnusamy, S. Harish, M. Navaneethan, *Controlled grain boundary interfaces of reduced graphene oxide in Ag_2Se matrix for low lattice thermal conductivity and enhanced power factor for thermoelectric applications*, *J Power Sources* **525** (2022) [doi.org/10.1016/j.jpowsour.2022.231045].

[41] X. Wang *et al.*, *Compound defects and thermoelectric properties in ternary CuAgSe-based materials*, *J Mater Chem A Mater* **3** (2015) [doi.org/10.1039/c5ta02721g].

[42] Genovese, C. Cocchiara, S. Piazza, C. Sunseri, and R. Inguanta, *Electrochemical deposition of Ag_2Se nanostructures*, *Mater Res Bull* **86** (2017), [doi.org/10.1016/j.materresbull.2016.09.033].

[43] T. Ohtani, K. Maruyama, K. Ohshima, *Synthesis of copper, silver, and samarium chalcogenides by mechanical alloying*, *Mater Res Bull* **32** (1997) [doi.org/10.1016/S0025-5408(96)00188-2].

[44] J. Chen *et al.*, *Hierarchical Structures Advance Thermoelectric Properties of Porous n-type β-Ag_2Se*, *ACS Appl Mater Interfaces* **12** (2020) [doi.org/10.1021/acsami.0c15341].

[45] Li, H. Feng, X. Wei, K. Jiang, S. Xue, P. K. Chu, *Ag as Cocatalyst and Electron-Hole Medium in CeO_2 QDs/Ag/Ag_2Se Z-scheme Heterojunction Enhanced the Photo-Electrocatalytic Properties of the Photoelectrode*, *Nanomaterials* **10** (2020) [doi.org/10.3390/nano10020253].

[46] D. Park, M. Kim, J. Kim, *Fabrication of PEDOT:PSS/Ag_2Se Nanowires for Polymer-Based Thermoelectric Applications*," *Polymers (Basel)* **12** (2020) [doi.org/10.3390/polym12122932].

[47] T. Li, S. Vongehr, S. Tang, Y. Dai, X. Huang, X. Meng, *Scalable Synthesis of Ag Networks with Optimized Sub-monolayer Au-Pd Nanoparticle Covering for Highly Enhanced SERS Detection and Catalysis*, *Sci Rep* **6** (2016) [doi.org/10.1038/srep37092].

[48] Nazemi, L. Soule, M. Liu, M. A. El-Sayed, *Ambient Ammonia Electrosynthesis from Nitrogen and Water by Incorporating Palladium in Bimetallic Gold–Silver Nanocages*, *J Electrochem Soc* **167** (2020) [doi.org/10.1149/1945-7111/ab6ee9].

[49] J. Firet, M. A. Blommaert, T. Burdyny, A. Venugopal, D. Bohra, A. Longo, W. A. Smith, *Operando EXAFS study reveals presence of oxygen in oxide-derived silver catalysts for electrochemical CO_2 reduction*, *J Mater Chem A Mater* **7** (2019) [doi.org/10.1039/c8ta10412c].

[50] J. Qu *et al.*, *Intraband Mid-Infrared Transitions in Ag_2Se Nanocrystals: Potential and Limitations for Hg-Free Low-Cost Photodetection*, *The Journal of Physical Chemistry C* **122 (**2018) [doi.ORG/10.1021/acs.jpcc.8b05699].

[51] F. Sun, Y. Li, Z. Wu, Y. Liu, H. Tang, X. Li, Z. Yuea, L. Zhou, *In situ reactive coating of metallic and selenophilic Ag_2Se on Se/C cathode materials for high performance Li–Se batteries*, *RSC Adv* **8** (2018) [doi.org/10.1039/C8RA06484A].